A magnetization and neutron powder diffraction study of $RFe_{9.5}Mo_{2.5}$ compounds (R = Y, Dy, Ho, Er)

1998 J. Phys.: Condens. Matter 10 4101

(http://iopscience.iop.org/0953-8984/10/18/019)

J. Phys.: Condens. Matter **10** (1998) 4101–4112. Printed in the UK PII: S0953-8984(98)88710-9

A magnetization and neutron powder diffraction study of $RFe_{9.5}Mo_{2.5}$ compounds (R = Y, Dy, Ho, Er)

J Ayres de Campos†, L P Ferreira‡, M Godinho§, J M Gil‡, P J Mendes‡, N Ayres de Campos‡, I C Ferreira†, M Bououdina‖, M Bacmann‖, J-L Soubeyroux‖, D Fruchart‖ and A Collomb‖

† Departamento de Física, Universidade do Minho, P-4719 Braga, Portugal
‡ Departamento de Física, Universidade de Coimbra, P-3000 Coimbra, Portugal
§ Departamento de Física, FCUL, Campo Grande, P-1700 Lisboa, Portugal
‖ Laboratoire de Cristallographie du CNRS, BP 166, F-38042 Grenoble Cédex 9, France

Received 27 October 1997, in final form 14 January 1998

Abstract. Neutron powder diffraction experiments and magnetic measurements were performed on compounds of the series $RFe_{9.5}Mo_{2.5}$ (R = Y, Dy, Ho and Er). The influence of the R element on both the structural and the magnetic properties of the different compounds is discussed, as well as the possible correlation between the iron environments and the local moments. Comparison is made with a previous Mössbauer study on the same compounds.

1. Introduction

The Fe-rich ternary compounds $RFe_{12-x}M_x$ (R = rare earth and M = Ti, V, Cr, Mo, Si) have been extensively studied in recent years due to their interest as possible candidates for permanent magnet applications [1]. These compounds crystallize in the tetragonal $ThMn_{12}$-type structure with space group $I4/mmm$ [2]. In this structure, the R atoms occupy the crystallographic 2a sites and the Fe atoms occupy the 8i, 8j and 8f sites. Usually, the M element substitutes for Fe atoms preferentially at the 8i sites [3], but different occupation sites have been found when M = Co, Si, Al and Ga [4–6].

In a recent study of the evolution with temperature of the magnetic behaviour of the $RFe_{9.5}Mo_{2.5}$ series (R = Y, Dy, Nd and Er) by Mössbauer spectroscopy [7], it was shown that modifications related to magnetic ordering occur over a broad range of temperatures and can be assigned differently to the three iron sites, contradicting the idea of a cluster-like magnetic behaviour occurring in compounds at Mo concentration $x = 2.0$ [8].

A systematic structural and magnetic study of the $RFe_{9.5}Mo_{2.5}$ compounds (R = Y, Dy, Ho and Er) using neutron diffraction and magnetization measurements is presented in this paper.

2. Experimental details

The $RFe_{9.5}Mo_{2.5}$ compounds with R = Y, Dy, Ho and Er were prepared by melting suitable quantities of the different elements (purity 99.99% (4N)) in a cold-crucible induction furnace under a 5N-purity argon atmosphere. In order to prevent excessive evaporation of the low-melting-point element R, a stoichiometric Fe–Mo alloy was melted as a first step, and in

0953-8984/98/184101+12$19.50

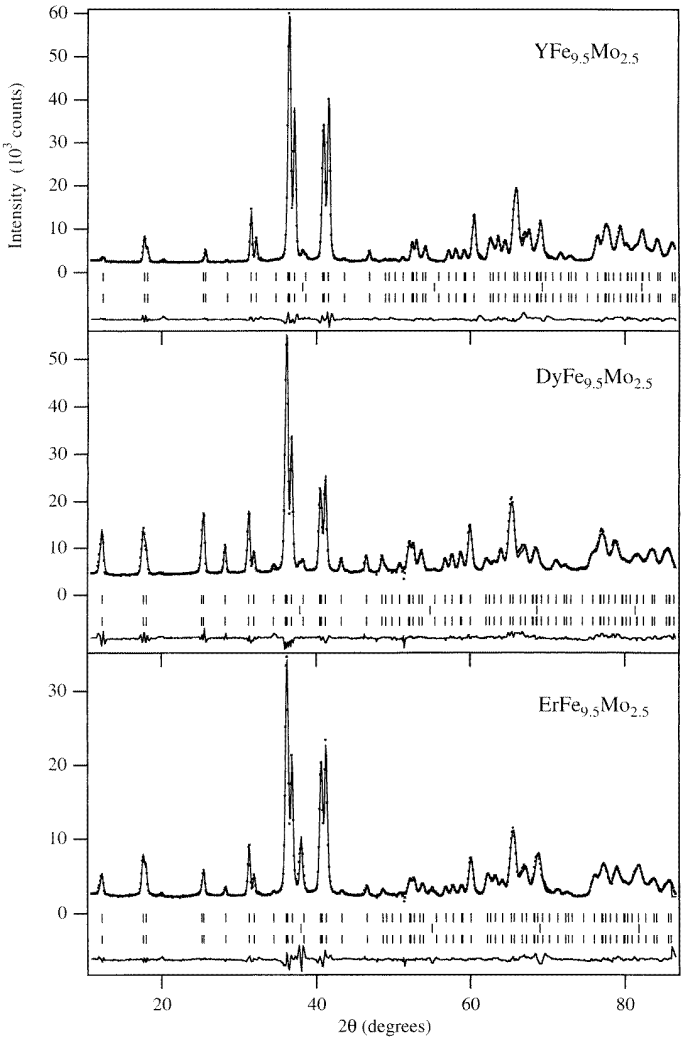

Figure 1. Experimental (dots) and calculated (lines) neutron diffraction diagrams for Y, Dy and Er samples at 6 K ($\lambda_n = 1.336$ Å). The difference pattern (observed − calculated) is shown in the bottom of each diagram. The short bars correspond to the nuclear peaks, the iron impurities and the magnetic peaks.

a second melting the R element was added. Afterwards, the samples were sealed in silica tubes filled with pure argon gas and annealed for ten days at temperatures close to 900 °C. That the tetragonal phase had been achieved was confirmed by x-ray powder diffraction. A small amount of α-Fe (or α-Fe(Mo)) is frequently observed as an impurity ($\leqslant$5 wt%).

Magnetic measurements on non-oriented powder samples were performed using a SQUID magnetometer over the temperature range 5 K to 400 K, under magnetic fields up to 5.5 T.

Neutron diffraction experiments were carried out at the Siloé reactor or at the ILL D1B diffractometer, in Grenoble, at 6 K and 290 K for each sample. The nuclear and magnetic structures were refined with the Rietveld method using the Fullprof program [9].

Table 1. Refined parameters and reliability factors derived from neutron diffractograms obtained at room temperature: n is the occupation number; x, y and z are the atom position coordinates; a and c are the lattice parameters; R_p is the profile factor and R_B is the Bragg factor.

Compound	Atom	n	x	y	z	a (Å)	c (Å)	R_p (%)	R_B (%)
$YFe_{9.5}Mo_{2.5}$	Y (2a)	2.0	0.0000	0.0000	0.0000	8.561(1)	4.808(1)	3.82	3.75
	Fe (8f)	8.0	0.2500	0.2500	0.2500				
	Fe (8i)	3.2(1)	0.3572(3)	0.0000	0.0000				
	Mo (8i)	4.8(1)	0.3572(3)	0.0000	0.0000				
	Fe (8j)	8.0	0.2823(3)	0.5000	0.0000				
$DyFe_{9.5}Mo_{2.5}$	Dy (2a)	2.0	0.0000	0.0000	0.0000	8.583(1)	4.819(1)	2.55	5.36
	Fe (8f)	8.0	0.2500	0.2500	0.2500				
	Fe (8i)	3.0(2)	0.3564(4)	0.0000	0.0000				
	Mo (8i)	4.9(2)	0.3564(4)	0.0000	0.0000				
	Fe (8j)	8.0	0.2825(4)	0.5000	0.0000				
$HoFe_{9.5}Mo_{2.5}$	Ho (2a)	2.0	0.0000	0.0000	0.0000	8.559(1)	4.807(1)	5.36	4.49
	Fe (8f)	8.0	0.2500	0.2500	0.2500				
	Fe (8i)	3.0(1)	0.3577(1)	0.0000	0.0000				
	Mo (8i)	5.0(1)	0.3577(1)	0.0000	0.0000				
	Fe (8j)	8.0	0.2833(1)	0.5000	0.0000				
$ErFe_{9.5}Mo_{2.5}$	Er (2a)	2.0	0.0000	0.0000	0.0000	8.557(1)	4.810(1)	2.37	2.61
	Fe (8f)	8.0	0.2500	0.2500	0.2500				
	Fe (8i)	2.7(1)	0.3572(3)	0.0000	0.0000				
	Mo (8i)	5.3(1)	0.3572(3)	0.0000	0.0000				
	Fe (8j)	8.0	0.2839(3)	0.5000	0.0000				

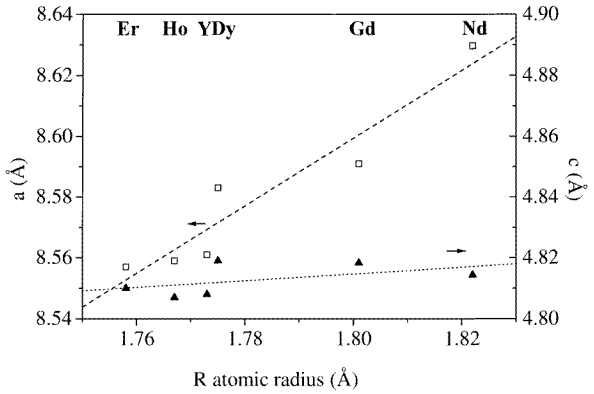

Figure 2. Lattice parameters refined from the neutron diffraction patterns measured at room temperature and plotted as a function of the atomic radius of the R element: a-parameter (□); c-parameter (○). The lines are linear regressions through the experimental points.

3. Results

3.1. Crystal structure

In figure 1, low-temperature neutron diffraction patterns are shown together with the fitted profiles. As expected, all of the patterns correspond to the tetragonal $ThMn_{12}$-type structure, with space group $I4/mmm$ and $Z = 2$, where Z is the number of formula units per cell.

The refined structure parameters for room temperature are given in table 1. Good fitting results were obtained with Mo atoms occupying the 8i sites only. As can be seen in table 1, the final occupation numbers n are in good agreement with the expected Mo concentrations. Small amounts of an iron-rich phase were seen, at percentages varying from 0.5% for the Y compound to less than 4% for the Ho compound. Figures 2 and 3 illustrate the evolution of the cell parameters, the cell volume and the c/a ratio measured at 290 K, versus the atomic radius [10] of the R elements. Structural data for the Nd and Gd samples obtained from x-ray diffraction [11] were added for comparison.

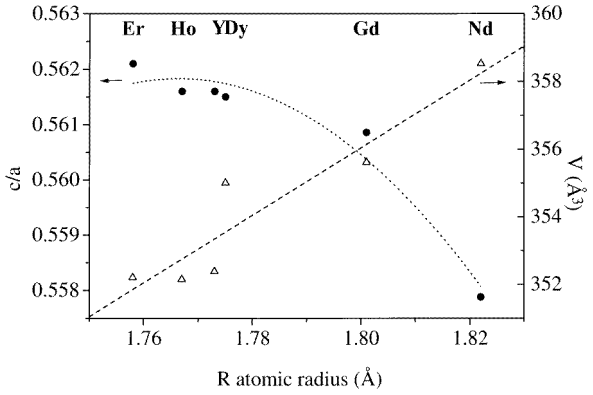

Figure 3. The c/a ratio (●) and lattice cell volume (△) plotted as a function of the atomic radius of the element R. The lines are guides to the eye.

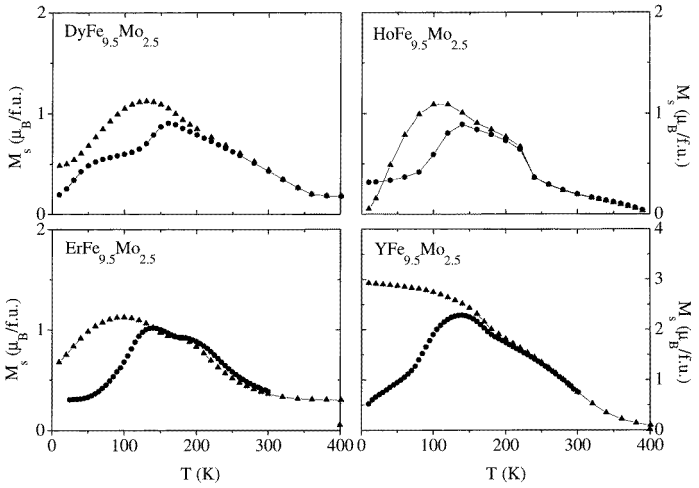

Figure 4. ZFC (●) and FC (500 Oe) (△) magnetization curves for $RFe_{9.5}Mo_{2.5}$.

Along the a-axis, the atoms are in close contact, following the sequence R–(Fe, Mo) 8i–(Fe, Mo) 8i–R; along the c-axis the R atoms are far from each other, separated by the octahedral 2b empty sites (the preferential site for hydrogen, carbon or nitrogen insertion). In fact, the cell parameter a shows the greatest variation, which explains the increase of the

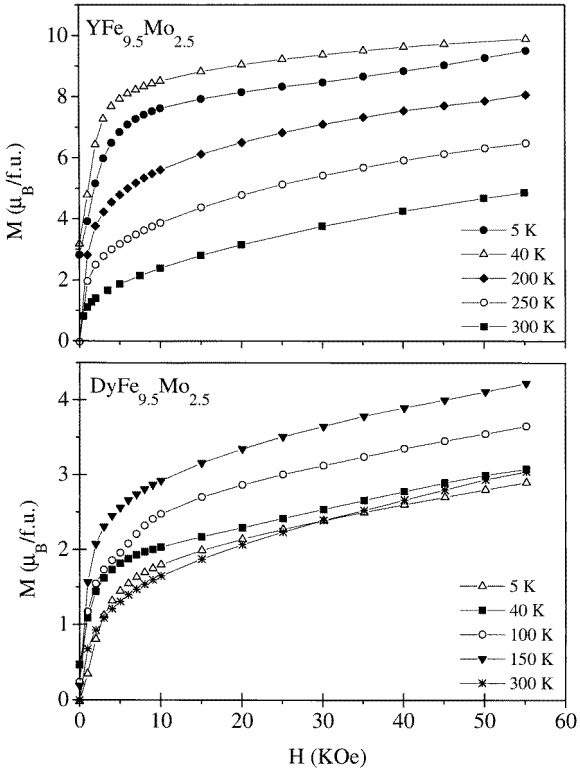

Figure 5. Magnetization measured as a function of H for Y and Dy samples.

c/a ratio seen in figure 3, and the corresponding cell volume variation, in good agreement with the expected lanthanide contraction.

3.2. Magnetic behaviour

3.2.1. Magnetization results. In figures 4–6 and in table 2, selected magnetization results for the compounds studied are presented.

In figure 4 the zero-field-cooled (ZFC) and field-cooled (FC) magnetization curves are shown. The ZFC and FC curves were obtained after cooling the samples from 400 K to 10 K under conditions of zero applied field and a measurement field of 500 Oe, respectively; in both cases the measurements were performed while increasing the temperature. The Curie temperatures obtained from the inflection points in the FC curves are presented in table 2. These values are in good agreement with the Mössbauer results for the same samples [7, 11].

The curves show distinct ZFC and FC magnetization values at low temperatures. For the FC curves different behaviours are detected for the four samples. For the Y compound, the highest magnetization value in the FC procedure is obtained at the lowest temperature (10 K) with the difference between the values of the ZFC and FC curves indicating an easy alignment of the fine powder grains along the applied-field direction. This corresponds to the orientation of the easy axis for iron, i.e. the c-axis (as confirmed from the neutron results discussed below), along the field direction. In contrast, for the other samples the highest magnetization values (FC curves) are reached at around 100 K, and at 10 K the magnetization

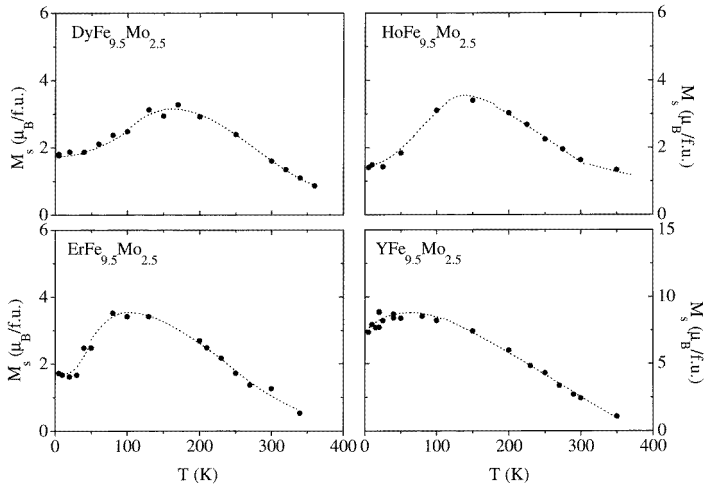

Figure 6. The temperature dependence of the spontaneous magnetization in $RFe_{9.5}Mo_{2.5}$. The lines are guides to the eye.

Table 2. Magnetic characteristics at 6 K: μ and θ are the magnetic moment and the moment orientation relative to *c*-axis, extracted from neutron diffraction analysis; m_n is the magnetization per formula unit calculated from neutron data; m_m and T_C are the magnetization per formula unit and the Curie temperature obtained from magnetic measurements; $\langle B_{hf} \rangle$ is the average hyperfine field measured by Mössbauer spectroscopy.

Compound	Atom (site)	μ (μ_B)	n	$\langle \mu_{Fe} \rangle$ (μ_B)	θ	m_n (μ_B/f.u.)	m_m (μ_B/f.u.)	T_C (K)	$\langle B_{hf} \rangle$ (T)
$YFe_{9.5}Mo_{2.5}$	Fe (8f)	0.9(1)	8.0	1.01(4)	0	10.8(3)	8.5	295(10)	14.5
	Fe (8i)	1.36(4)	3.2(1)						
	Fe (8j)	1.0(1)	8.0						
$DyFe_{9.5}Mo_{2.5}$	Dy (2a)	−8.3(1)	2.0	1.22(7)	−8(1)	4.6(1.4)	1.8	330(10)	12.5
	Fe (8f)	1.09(7)	8.0						
	Fe (8i)	1.3(2)	3.1(2)						
	Fe (8j)	1.3(1)	8.0						
$HoFe_{9.5}Mo_{2.5}$	Ho (2a)	−9.1(9)	2.0	0.88(6)	0	0.2(1.0)	1.4	240(10)	11.6
	Fe (8f)	0.80(5)	8.0						
	Fe (8i)	0.9(5)	3.0(1)						
	Fe (8j)	0.94(6)	8.0						
$ErFe_{9.5}Mo_{2.5}$	Er (2a)	−4.8(1)	2.0	0.67(8)	−16(3)	2.5(1.7)	1.6	230(10)	11.5
	Fe (8f)	0.62(8)	8.0						
	Fe (8i)	0.8(3)	2.7(1)						
	Fe (8j)	0.7(1)	8.0						

is found to be only slightly higher (the Dy and Er compounds) or even smaller (the Ho compound) than the corresponding values for the ZFC curves. This behaviour is certainly related to the antiparallel alignment of the rare-earth and iron moments for temperatures below 100 K. Above this temperature only the Fe sublattice contributes to the magnetization.

The magnetization was also measured as a function of the applied field, for fields up to 5.5 T, for all of the samples. A ferromagnetic-type behaviour, without saturation up

to the highest applied field, is observed in all cases. The $M(H)$ variation for the Y and Dy samples is shown in figure 5. In general the magnetization values for all temperatures at the highest field agree with the values obtained for the $M(T)$ curves. In the case of Y there is a net decrease of the spontaneous magnetization for temperatures lower than 30 K. This behaviour is not detected in the temperature variation of the magnetization, or in the neutron powder diffraction result at 6 K, but a small anomaly was observed in the a.c. susceptibility curves in this temperature range [7]. This may suggest some degree of non-collinear arrangement of Fe moments at low temperatures.

Figure 6 shows the spontaneous magnetization (M_S) obtained by extrapolating to $H = 0$ the behaviour observed at the higher fields on each magnetization isotherm. The magnetic moments per formula unit presented in table 2 (m_m) were determined from the magnetization values at 5 K.

3.2.2. Neutron diffraction results. The R and Fe magnetic moments deduced from neutron diffraction analysis at 6 K are reported in table 2. As can be noticed, the magnetic structures of the Dy, Ho and Er compounds are ferrimagnetic, with the rare-earth moment aligned antiparallel to the iron moments. This agrees with both the $J = L + S$ coupling rule for the heavy rare-earth elements and the 3d–4f negative-spin-coupling scheme [12, 13].

The Y alloy shows magnetic moments collinear with the *c*-axis, as expected from the zero magnetic moment of Y. The Ho alloy also shows magnetic moments parallel to the *c*-axis, as a result of both a small and negative second-order crystal-field parameter associated with a small negative α_j-value [12] and the Fe-sublattice anisotropy along the *c*-axis. For the Dy ($\alpha_j < 0$) and Er ($\alpha_j > 0$) compounds, weak deviations between the direction of the iron moments and the *c*-axis were detected (table 2). From the results obtained for the $RFe_{10.5}Mo_{1.5}$ parent series [14], it was predictable that intermediate orientations of the iron magnetic moments should occur; however, in the former series, the angular deviation from the *c*-axis for the Dy and Er compounds was found to be larger ($\approx 60^\circ$). Since the R element has four 8i sites as first neighbours and the Mo concentration at these sites increases from 37.5% in the $Mo_{1.5}$ series to 62.5% in the $Mo_{2.5}$ series, comparison with our results suggests that an increase in the Mo concentration weakens the crystal field at the R site and/or reduces the R–R and R–Fe exchange interactions.

The Mo content could also explain the measured R magnetic moment, which is smaller than the saturation moment of R^{3+}. In fact, the Mo-atom distribution close to the 2a sites could break down the magnetic exchange couplings within the R sublattice to some extent, consequently weakening its contribution to the neutron magnetic scattering.

4. Discussion

4.1. Iron moments and the atomic environment

From table 2, the relationship between the different iron moments, as measured at 10 K, can be given as follows: $\mu(8i) \geqslant \mu(8j) > \mu(8f)$. This trend has already been found in the $RFe_{10.5}Mo_{1.5}$ series [14], and seems to be reasonable if one considers the atomic environment of each iron site.

Considering the numbers of iron nearest neighbours (NN), it can be seen in table 3 that the iron atoms on 8i sites have 10.5 iron NN, while iron atoms on both 8f and 8j sites have only 7.5 iron NN (62.5% of the 8i sites are occupied by Mo atoms in these samples). Local polarization effects related to the coordination number could thus explain the larger 8i iron moment. Besides, taking into account the ⟨Fe–Fe⟩ distances reported

Table 3. Interatomic distances (d) and numbers of nearest neighbours (NN) for $RFe_{9.5}Mo_{2.5}$ compounds.

	NN	Atoms	d (Å) Dy	d (Å) Ho	d (Å) Y	d (Å) Er
R (2a)	8	Fe (8f)	3.2628(2)	3.2537(1)	3.2543(1)	3.2541(3)
	8	Fe (8j)	3.055(3)	3.0604(1)	3.045(2)	3.036(3)
	4	(Fe, Mo) (8i)	3.065(3)	3.090(9)	3.064(3)	3.055(4)
Fe (8f)	2	Fe(8f)	2.4073(3)	2.4008(1)	2.401(2)	2.4029(3)
	4	Fe (8j)	2.473(4)	2.464(9)	2.467(2)	2.469(4)
	4	(Fe, Mo) (8i)	2.626(3)	2.630(8)	2.621(2)	2.618(4)
	2	R (2a)	3.2628(2)	3.2537(1)	3.2543(1)	3.2541(3)
Fe (8j)	4	Fe (8f)	2.4732(5)	2.464(1)	2.4672(3)	2.4691(6)
	2	Fe (8j)	2.660(4)	2.68(1)	2.647(3)	2.624(4)
	2	(Fe, Mo) (8i)	2.701(5)	2.680(6)	2.695(3)	2.713(5)
	2	(Fe, Mo) (8i)	2.683(2)	2.66(1)	2.681(2)	2.686(3)
	2	R (2a)	3.055(3)	3.0604(1)	3.045(2)	3.036(3)
(Fe, Mo) (8i)	4	Fe (8f)	2.626(1)	2.630(3)	2.6213(9)	2.618(2)
	2	Fe (8j)	2.683(2)	2.659(6)	2.681(2)	2.686(3)
	2	Fe (8j)	2.701(3)	2.680(6)	2.695(2)	2.713(3)
	1	(Fe, Mo) (8i)	2.448(5)	2.37(1)	2.428(4)	2.445(6)
	4	(Fe, Mo) (8i)	2.965(2)	2.930(5)	2.952(2)	2.960(3)
	1	R (2a)	3.065(3)	3.090(9)	3.064(3)	3.055(4)

in table 3, the calculated average values for distances between the iron atoms at 8f, 8j and 8i sites and their neighbours are found to be close to 2.5, 2.6 and 2.7 Å respectively. These average interatomic distances follow the trend exhibited by the Wigner–Seitz (W–S) cell volumes of the 3d-metal sites calculated for the pseudo-binary $R(FeM)_{12}$ compounds, $V(8i) > V(8j) > V(8f)$ [15], and a direct relationship with the iron local moments reported in table 2 can be established. Shorter interatomic distances around the iron atom (smaller W–S volumes) would correspond to smaller iron moments. In other words, the local iron moments should be related to the degree of orbital overlap with the surrounding atoms.

4.2. Iron moments and Mössbauer hyperfine fields

Figure 7(a) shows the average iron magnetic moments for the $RFe_{9.5}Mo_{2.5}$ series, calculated from the μ-values given in table 2. The mean values of the iron magnetic moments deduced from neutron diffraction experiments performed on (Dy, Er)$Fe_{10.5}Mo_{1.5}$ are also plotted [14]. Through the two series a similar increase of the mean iron moments with increasing radius of R is observed. Between the 1.5 and 2.5 series a mean drop of the iron moment values close to 0.9 μ_B can be observed.

Figure 7(b) presents the average hyperfine fields obtained by Mössbauer spectroscopy for the $RFe_{9.5}Mo_{2.5}$ compounds [7]. The dashed line in the same figure represents the least-squares fitting to the iron moments of the $x = 2.5$ series shown in figure 7(a). For the samples with Dy, Ho and Er (magnetic R), a mean value of 11.9 ± 0.6 T can be calculated for $\langle B_{hf} \rangle$ (solid line). Generally it is found that for the Y–Fe systems the average hyperfine field is proportional to the average Fe moment, and a coefficient around 15 T/μ_B has been obtained [8, 16–18]. From figure 7(b) the value 15.9 T/μ_B is found for $YFe_{9.5}Mo_{2.5}$.

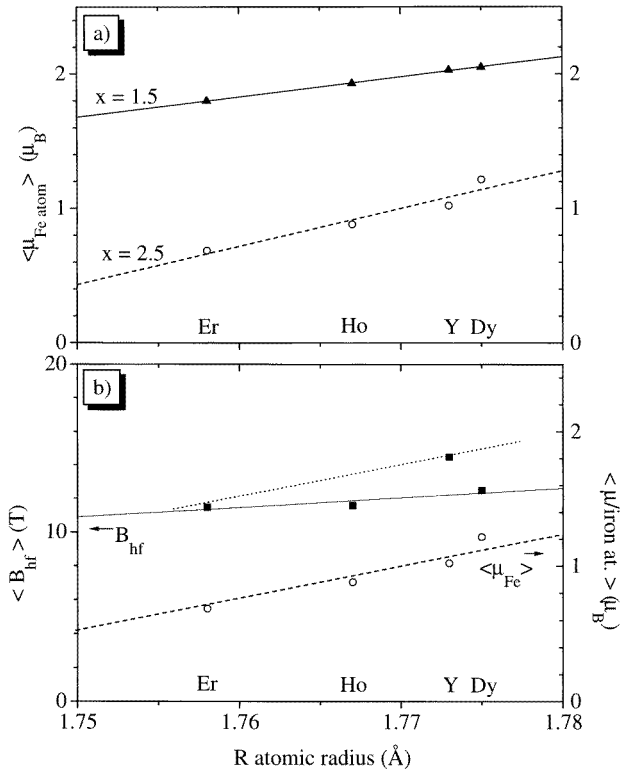

Figure 7. (a) The average iron moment plotted as a function of the atomic radius of R for the $RFe_{9.5}Mo_{2.5}$ (○) and $RFe_{10.5}Mo_{1.5}$ (▲) series. (b) The average hyperfine field of iron plotted as a function of the atomic radius of the R element (■) for $RFe_{9.5}Mo_{2.5}$. The dashed line represents the average iron moment also plotted in (a). The dotted line, parallel to the dashed line, represents the Fe magnetic contribution for the hyperfine field. The solid line is a linear regression through the $\langle B_{hf}\rangle$ values measured for the samples with magnetic R elements.

In the Y compound the hyperfine-field magnetic contribution comes only from the Fe sublattice. However, for Dy, Ho and Er compounds the transferred field arises also from the magnetic R atoms. If just the Fe contribution were present, $\langle B_{hf}\rangle$ for all of the samples should be well fitted by the dotted line that goes through the Y $\langle B_{hf}\rangle$ value. (This dotted line has the same slope as the dashed line for the moments, assuming a linear relation between $\langle B_{hf}\rangle$ and $\langle \mu_{\mathrm{Fe}}\rangle$.) Therefore, the difference between the experimental $\langle B_{hf}\rangle$ values and the corresponding values in the dotted line is a measure of the R magnetic transferred-field contribution, leading to a mean value around 1.6 T, in good agreement with the literature [19].

4.3. Iron moments and the Curie temperature

In figure 8(a), the Curie temperatures of the $RFe_{12-x}Mo_x$ compounds for $x = 1.5$ and 2.5 are plotted. The decreases of T_C with the atomic radius of R are found to be approximately the same for the two series. Assuming a linear dependence on the Mo concentration, a mean value of 130 K/Mo is found for the T_C-drop from the $x = 1.5$ to the $x = 2.5$ compounds, leading to a value of T_C of around 650 K for the hypothetical YFe_{12}.

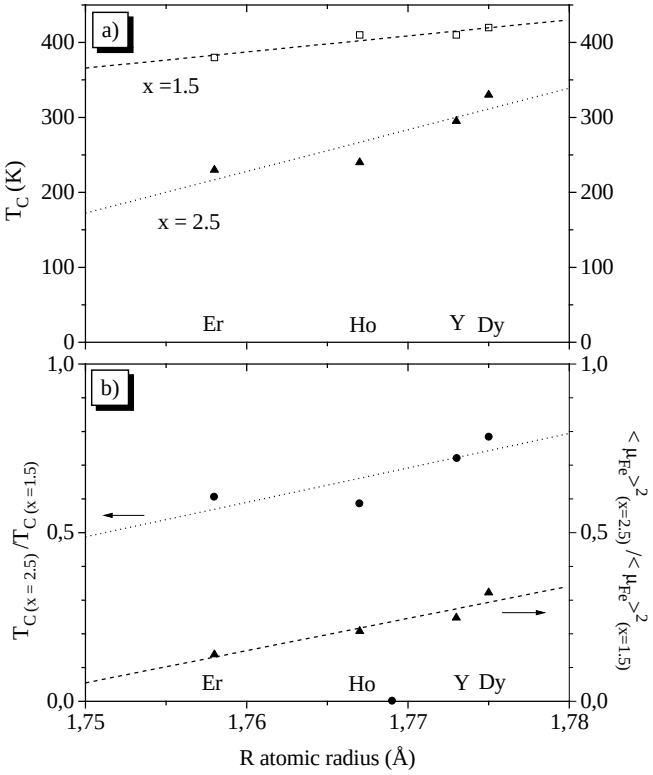

Figure 8. (a) The Curie temperatures of the $RFe_{12-x}Mo_x$ compounds with R = Dy, Y, Ho, Er for $x = 1.5$ (□) and $x = 2.5$ (▲) as a function of the atomic radius of R. The lines are linear regressions through the experimental points. (b) The ratios $T_C(x = 2.5)/T_C(x = 1.5)$ (●) and $\langle\mu_{Fe}\rangle^2(x = 2.5)/\langle\mu_{Fe}\rangle^2(x = 1.5)$ (▲) versus the atomic radius of the R element. The lines are linear regressions through the experimental points.

From the molecular-field approximation, the Curie temperature can be expressed [20] as follows:

$$T_C = \frac{T_{Fe}}{2} + \sqrt{\left(\frac{T_{Fe}}{2}\right)^2 + T_{RFe}^2} \tag{1}$$

with

$$\begin{aligned} T_{Fe} &= \frac{4N_{Fe}}{3k_B} n_{Fe}\mu_B^2 S_{Fe}(S_{Fe}+1) \\ T_{RFe}^2 &= \frac{16N_R N_{Fe}}{9k_B^2} n_{RFe}^2 \mu_B^4 S_{Fe}(S_{Fe}+1) G_J \end{aligned} \tag{2}$$

where N_i is the i-sublattice number of atoms in the volume unit, $G_J = (g_J - 1)^2 J(J+1)$ is the de Gennes factor and S_{Fe} is the effective spin moment of iron ($\langle\mu_{Fe}\rangle = -2S_{Fe}\mu_B$). The molecular-field parameters are related to the interatomic exchange coupling terms as follows:

$$n_{Fe} = \frac{Z_{FeFe}}{2N_{Fe}\mu_B^2} J_{FeFe} \qquad \text{and} \qquad n_{RFe}^2 = \frac{Z_{RFe}Z_{FeR}}{16N_R N_{Fe}\mu_B^2} J_{RFe}^2 \tag{3}$$

where Z_{AB} is the number of B first neighbours of the atom A.

From equation (1), it can be seen that the T_{Fe}-contribution to T_C is dominant. Thus figures 7(a) and 8(a) allow us to conclude that both $\langle\mu_{Fe}\rangle$ and the $\langle J_{Fe}\rangle$ exchange parameter are markedly reduced when x changes from 1.5 to 2.5 Mo/f.u. and both decrease through the R series. In figure 8(b), it can be seen that the $T_C(2.5)/T_C(1.5)$ curve mimics the variation of $\langle\mu_{Fe}\rangle^2(2.5)/\langle\mu_{Fe}\rangle^2(1.5)$ with the R atomic radius, according to equation (2).

From figure 8(a), the T_C-values of the two series decrease in a similar way with the radius of R which means that the coupling J_{RFe} exchange term (the de Gennes contribution to T_C) does not vary appreciably when passing from $x = 1.5$ to $x = 2.5$. However, since the slope for the 2.5 series is slightly higher than that for the 1.5 series, a higher contribution of the R–Fe term to T_C in the 2.5 series can be inferred.

5. Conclusions

From the iron hyperfine field measured in the $RFe_{9.5}Mo_{2.5}$ compounds, a mean value of 1.6 T was inferred for the R magnetic transferred-field contribution. A strong reduction in the $\langle J_{Fe}\rangle$ exchange parameter is observed when the Mo content varies from 1.5 to 2.5, but the J_{RFe} exchange terms are similar for the two series. A larger contribution of the R–Fe term to T_C can be deduced for the 2.5 series.

The coordination number for each iron site, the ⟨Fe–Fe⟩ distances and the degree of orbital overlap seem to be the most important factors determining the local iron moments. Changes which affect the iron properties (iron local moments, Fe–Fe exchange interactions) are responsible for the observed changes in the net magnetization and Curie temperature of the series $RFe_{12-x}Mo_x$, R = Y, Dy, Ho, Er. Further experiments are planned in order to check the validity of this conclusion using compounds containing light rare-earth elements ($J = L - S$).

Acknowledgments

This study was partly funded by the Portuguese–French JNICT–CNRS collaboration and by the EEC-HCM scheme of grants.

References

[1] Li H S and Coey J M D 1993 *Handbook of Magnetic Materials* vol 6, ed K H J Buschow (Amsterdam: North-Holland) p 1
[2] Florio J V, Rundle R E and Snow A I 1952 *Acta Crystallogr.* **5** 449
[3] Buschow K H J 1988 *J. Appl. Phys.* **63** 3130
[4] Mooij D B and Buschow K H J 1988 *J. Less-Common Met.* **136** 207
[5] Christides C, Anagnostou M, Li Hong-Shuo, Kostikas A and Niarchos D 1991 *Phys. Rev.* B **44** 5
[6] Suski W 1995 *J. Alloys Compounds* **223** 237
[7] Ayres de Campos J, Gil J M, Mendes P J, Ferreira L P, Ferreira I C, Ayres de Campos N, Estrela P, Godinho M, Bououdina M, Collomb A, Fruchart D, Soubeyroux J-L, Takele S, Pelloth J and Brand R A 1996 *J. Magn. Magn. Mater.* **164** 305
[8] Christides C, Kostikas A, Zouganelis G, Psyharis V, Kou X C and Grössinger R 1993 *Phys. Rev.* B **47** 11 220
[9] Rodriguez-Carvajal J 1990 *Satellite Mtg of the 15th Congress of the IUCr (Toulouse)* abstracts, p 127
[10] Teatum E T, Gschneidner K A Jr and Waber J T 1968 Compilation of calculated data useful in predicting metallurgical behaviour of the element in binary alloy systems *Los Alamos, Scientific Laboratory of the University of California, Report* LA-4003, UC-25
[11] Ayres de Campos J 1998 *Thesis* Minho University, Portugal, to be published
[12] Hu Bo-Ping, Li Hong-Shuo and Coey J M D 1989 *J. Phys.: Condens. Matter* **1** 755

[13] Buschow K H J 1991 *J. Magn. Magn. Mater.* **100** 79
[14] Tomey E P 1994 *Thesis* Université Joseph Fourier, Grenoble
[15] Isnard O and Fruchart D 1994 *J. Alloys Compounds* **205** 1
[16] Gubbens P C M, van Apedoorn J H F, van der Kraan A M and Buschow K H J 1974 *J. Phys. F: Met. Phys.* **4** 921
[17] Sinnemann Th, Erdmann K, Rosenberg M and Buschow K H J 1988 *Hyperfine Interact.* **40** 389
[18] Obbade S 1991 *Thesis* Université Joseph Fourier, Grenoble
[19] Li Z W, Zhou X Z and Morrish A H 1992 *J. Phys.: Condens. Matter* **4** 10 409
[20] Herbst J F 1991 *Rev. Mod. Phys.* **63** 819